

Novel 3D Lung Tumor Spheroids for Oncoimmunological Assays

Kirsten De Ridder, Navpreet Tung, Jan-Timon Werle, Léa Karpf, Robin Maximilian Awad, Annie Bernier, Hannelore Ceuppens, Hélène Salmon, and Cleo Goyvaerts*

Lung cancer thrives in a complex multicellular tumor microenvironment (TME) that impacts tumor growth, metastasis, response, and resistance to therapy. While orthotopic murine lung cancer models can partly recapitulate this complexity, they do not resonate with high-throughput immunotherapeutic drug screening assays. To address the current need for relevant and easy-to-use lung tumor models, a protocol is established to generate and evaluate fully histocompatible murine and human lung tumor spheroids, generated by coculturing lung fibroblasts with tumor cells in ultralow adherence 96-well plates. A spheroid generation protocol with the murine Kras^{G12D}p53^{-/-} (KP) and Lewis Lung Carcinoma (LLC) cell lines is delivered next to the human lung H1650 adenocarcinoma line. In addition, their application potential to study tumor-stroma organization, T-cell motility, and infiltration as well as distinct macrophage subsets' behavior using confocal microscopy is described. Finally, a 3D target-specific T-cell killing assay that allows spatiotemporal assessment of different tumor to T-cell ratios and immune checkpoint blockade regimens using flow cytometry and live cell imaging is described. This 3D lung tumor spheroid platform can serve as a blueprint for other solid cancer types to comply with the need for straightforward murine and human oncoimmunology assays.

efforts of ongoing research aim to identify predictive biomarkers and novel drug targets within the TME that can synergize with immunotherapy to improve therapeutic response rates.^[2]


Clinically approved immune checkpoint inhibitors (ICIs) to treat non-small-cell lung carcinoma (NSCLC) currently focus on the Programmed Death 1 (PD-1) pathway. Specifically, monoclonal antibodies against PD-1 or its ligand PD-L1 are administered to unleash cytotoxic T-cell lymphocyte (CTL)-mediated tumor elimination. Both tumor mutational burden and the PD-L1 expression levels are considered important predictive biomarkers for response to ICI.^[3,4] In search for novel biomarkers and drug targets, the spotlight has shifted to the TME which is composed of a heterogeneous collection of nonmalignant cells of hematopoietic and nonhematopoietic origin.^[5–7] The immunological landscape of lung cancers has been linked to the exclusion of cytolytic natural killer (NK) cells and cross-presenting dendritic

cells, next to an enrichment of B cells, nonfunctional (granzyme B⁻) T cells, and Foxp3⁺ regulatory T cells (Tregs).^[5,6,8–13] Together with the abundance of immunosuppressive myeloid cells such as neutrophils and tumor-associated macrophages (TAMs) with an M2-like protumoral profile, this immunological landscape has been shown to hamper ICI effectiveness.^[14,15] Similarly, mesenchymal cells, particularly cancer-associated fibroblasts (CAFs), have been described to facilitate extracellular matrix (ECM) remodelling and deposition as well

1. Introduction

In marked contrast to conventional treatments, immunotherapy does not target tumor cell division directly, but blocks immunosuppressive checkpoints that are heterogeneously expressed throughout the complex lung tumor microenvironment (TME). Although T-cell-based immunotherapy revolutionized the treatment paradigm for advanced lung cancer patients,^[1] this only holds true for a minor subset of patients. Thus, international

K. De Ridder, R. M. Awad, H. Ceuppens, C. Goyvaerts
Laboratory for Molecular and Cellular Therapy
Department of Biomedical Sciences
Vrije Universiteit Brussel
Laarbeeklaan 103-E, 1090 Jette, Belgium
E-mail: cleo.goyvaerts@vub.be

 The ORCID identification number(s) for the author(s) of this article can be found under <https://doi.org/10.1002/anbr.202100124>.

© 2021 The Authors. Advanced NanoBiomed Research published by Wiley-VCH GmbH. This is an open access article under the terms of the Creative Commons Attribution License, which permits use, distribution and reproduction in any medium, provided the original work is properly cited.

DOI: 10.1002/anbr.202100124

N. Tung, L. Karpf, H. Salmon
Department of Oncological Sciences
The Precision Immunology Institute
The Tisch Cancer Institute
Icahn School of Medicine at Mount Sinai
1470 Madison Avenue, New York, NY 10029, USA

J.-T. Werle, A. Bernier, H. Salmon
Institut Curie
INSERM
75005 Paris, France

J.-T. Werle, A. Bernier, H. Salmon
PSL Research University
75006 Paris, France

as immunomodulation resulting in T-cell exclusion from the tumor nest and accumulation in the CAF-rich stroma, that strongly correlates with poor responses to ICI.^[16–20] Although this complexity holds tremendous potential to unravel additional biomarkers and druggable targets for immunotherapy, high-throughput research is currently hampered by the lack of easy-to-use multicellular models that resemble human NSCLC histopathology.

Recently, 3D spheroid and organoid culture methods gained a lot of interest in the field of cancer biology, immuno-oncology, target discovery, and drug screening.^[21–24] Especially as they show a more heterogeneous morphology and proliferation rate compared to their monolayer 2D counterparts.^[25–29] While spheroids are typically generated using differentiated cancer cell lines, tumor organoids are derived from animal- or patient-derived progenitor cells found within isolated tumors. In addition, both can be cultured within semisolid scaffolds such as matrigel, or as suspensions inside low adherence plates or microfluidic chips. The latter offer an additional layer of physiological complexity, exemplified by their potential to monitor and regulate the laminar flow, fluid pressure, oxygen and/or nutrient supplies.^[30] Pioneering research by Sutherland et al. suggested that allo-specific splenocytes could infiltrate murine cancer spheroids and kill tumor cells.^[31] Moreover, it was shown that heterotypic 3D spheroids show a significantly lower yet more relevant capacity to be infiltrated and killed by murine and human CTLs.^[22,32–34] Finally, CAFs as well as myeloid cells have been evaluated using tumor spheroids to unravel direct and indirect tumor progression cues.^[22,35–39] Despite these reports, the use of lung tumor spheroids for immunotherapeutic research purposes have not been widely explored. This is partly attributed to most studies requiring technically challenging systems that require tools such as specific microfluidic devices, stirred tank vessels, alginate encapsulation or rail-based microstructures for hydrogel patterning. Furthermore, most 3D coculture assays use synthetic matrices such as collagen gels or matrigel, which do not resemble the ECM as it is produced by CAFs *in vivo*. Finally, the need for a completely histocompatible multicellular model, poses challenges on the generation of human 3D oncoimmunology models.

In this study, we describe a protocol to generate murine and human lung tumor spheroids that is uncomplicated, reproducible and has high-throughput read-out potential to assess antitumor immunity. We demonstrate that an optimized mixture of histocompatible lung fibroblasts with fluorescently labelled lung tumor cells organizes into coherent 3D aggregates with tumor nests surrounded by an ECM-producing fibroblastic stroma similar to the architecture observed in human lung tumor samples. Upon the addition of immune components abundant within the TME such as CD8⁺ T cells, MHC-II^{high} and/or MHC-II^{low} TAMs, we quantified localization, motility and overall immune phenotypes. Furthermore, we report on a murine and human 3D antigen-specific CTL killing assay to evaluate the spatiotemporal impact of CAFs, CTLs and/or TAM profiles during immunotherapeutic treatment.

2. Results

2.1. Lung Tumor Spheroids Recapitulate the Stromal Architecture of Human NSCLC

To generate murine lung cancer spheroids, we evaluated two commonly used murine lung cancer cell lines with C57BL/6 background (H2-Kb), the Kras^{G12D}p53^{-/-} (KP) and the Lewis lung carcinoma (LLC) cell lines^[40,41] while the human HLA-A2⁺ PC-9 and H1650 tumor lines were used for human lung cancer spheroid formation. Each tumor cell line was transduced with an enhanced Green Fluorescent Protein (eGFP)-encoding lentivector and further enriched for eGFP positivity using fluorescently labeled cell sorting (FACS) for tumor cell detection. To generate syngeneic murine fibroblasts, primary lung fibroblasts were isolated and immortalized via lentiviral introduction of SV40 large-T-antigen. Their fibroblast identity was confirmed by their significant expression of seven fibroblast-characterizing markers: alpha smooth muscle actin (α -SMA or ACTA2), S100A4, fibroblast activating protein (FAP), vimentin (VIM), podoplanin (PDPN), collagen type I alpha 1 chain (COL1A1) and platelet-derived growth factor receptor-beta (PDGFRB) (Figure S1 and Table S1, Supporting Information). The human IMR-90 (ATCC CCL-186) lung fibroblast line was obtained from ATCC.

We first aimed to define optimal tumor:fibroblast ratios, for which inclusion criteria were spheroid rigidity, volume uniformity, and tumor cell islet formation. Well-formed KP, LLC and H1650 3D spheroids were obtained 12 h after tumor cells were mixed with syngeneic fibroblasts at 3:5, 6:5, and 6:5 ratios, respectively (Figure 1A). As observed in a representative example of tumor cell (keratin+) and activated CAF (alpha smooth muscle actin, α SMA+) staining in a formalin-fixed, paraffin-embedded tumor from a lung cancer patient, human NSCLC tumors are organized in tumor islets surrounded by a CAF-rich stroma^[42](Figure 1B). To evaluate the tumor-stroma architecture in each type of tumor-CAF 3D coculture, 3-day old spheroids were formalin-fixed, frozen, and cryosectioned prior to staining of α -SMA. Confocal images revealed that eGFP⁺ cancer cells' organization into tumor nests was most pronounced for KP and H1650 spheroids, while CAFs and tumor cells showed a more mixed profile in LLC spheroids (Figure 1C). Notably, activated fibroblasts produced their own matrix in the co-culture, as observed with fibronectin fiber staining in the three types of spheroids (Figure 1D). Of note, whereas the KP and H1650 spheroids show a clear distinction between the fibronectin fibers and cancer cells, there is an overlapping fibronectin signal found on the membrane of eGFP⁺ LLC cells, suggestive for the mesenchymal character of the LLC cell line as previously described.^[43]

Finally, we evaluated the growth patterns of KP, LLC and H1650 spheroids, by monitoring their diameter (mm²) over a period of 25 days using EVOS fluorescence microscopy. The KP and H1650 spheroids showed a similar growth profile in which their diameters remained unchanged during the first 10 days before they expanded to maximum sizes of 200–400 μ m. LLC spheroids deviated from this pattern as their expansion already started 5 days after formation, resulting in 10 \times larger spheroids by day 25 (Figure 1E).

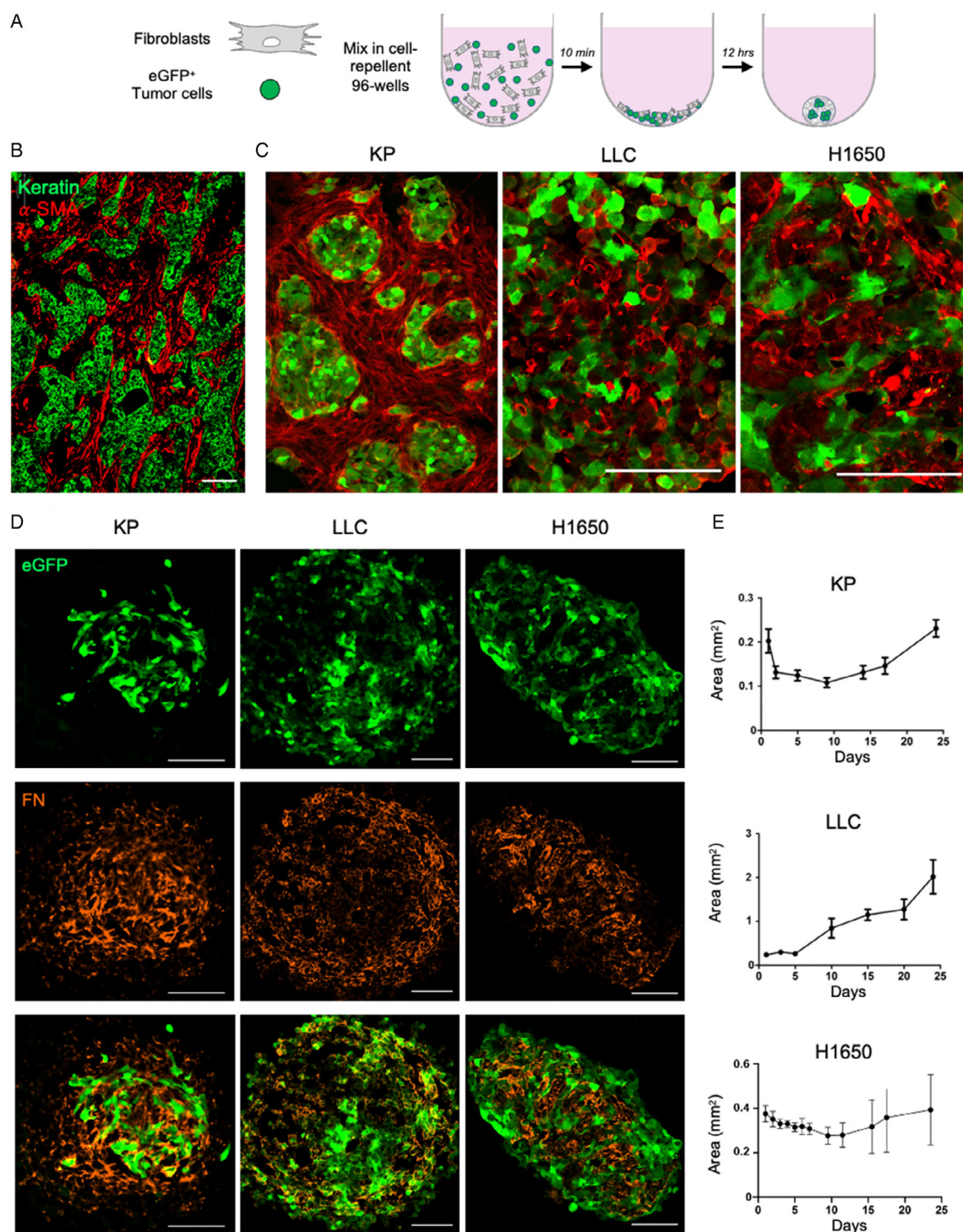


Figure 1. Lung tumor spheroid generation, organization and growth. A) Murine or human lung fibroblasts were mixed with eGFP⁺ KP, LLC or H1650 target cells at 5:3, 5:6, and 5:6 ratios respectively at 100 μ L medium/well of 96-well ultralow adherence (ULA) plates. B) Multiplexed immunohistochemical staining, performed on a formalin-fixed, paraffin-embedded human lung cancer biopsy. Sequential immunostainings for keratin (tumor cells, green) and α -SMA⁺ CAFs (red) were overlaid in pseudofluorescence. C and D) Confocal microscopy images of a representative formalin-fixed and frozen 3-day old KP (left), LLC (middle) and H1650 (right) spheroid. C) Overlay of eGFP⁺ cancer cells (green) and α -SMA⁺ CAFs (red). D) From top to bottom: distribution of eGFP⁺ cancer cells (green), fibronectin⁺ ECM (orange), and overlay of both channels. E) Sizes of KP, LLC and H1650 spheroids (generated with 5 k fibroblasts), were followed for 25 days, starting 12 h after their formation using the EVOS FL Auto Imaging System. Spheroid diameters (mm²) were calculated with ImageJ software ($n = 3$, 3 spheroids/experiment). Scale bars represent 100 μ m in all images.

2.2. Spheroids Allow Assessment of Immune Subset-Specific Infiltration Patterns

When evaluating specific knock-out models or immunotherapeutic agents, researchers may be interested in immune cell localization and motility properties within the TME.

As our KP spheroid system recapitulates the architecture of human NSCLC with tumor islets surrounded by CAFs, we wondered whether it could be a suitable model to study T-cell infiltration and motility (**Figure 2A**). Within a formalin-fixed, paraffin-embedded tumor sample from a lung cancer patient, CD3⁺ T cells showed a tumor-excluded profile where they

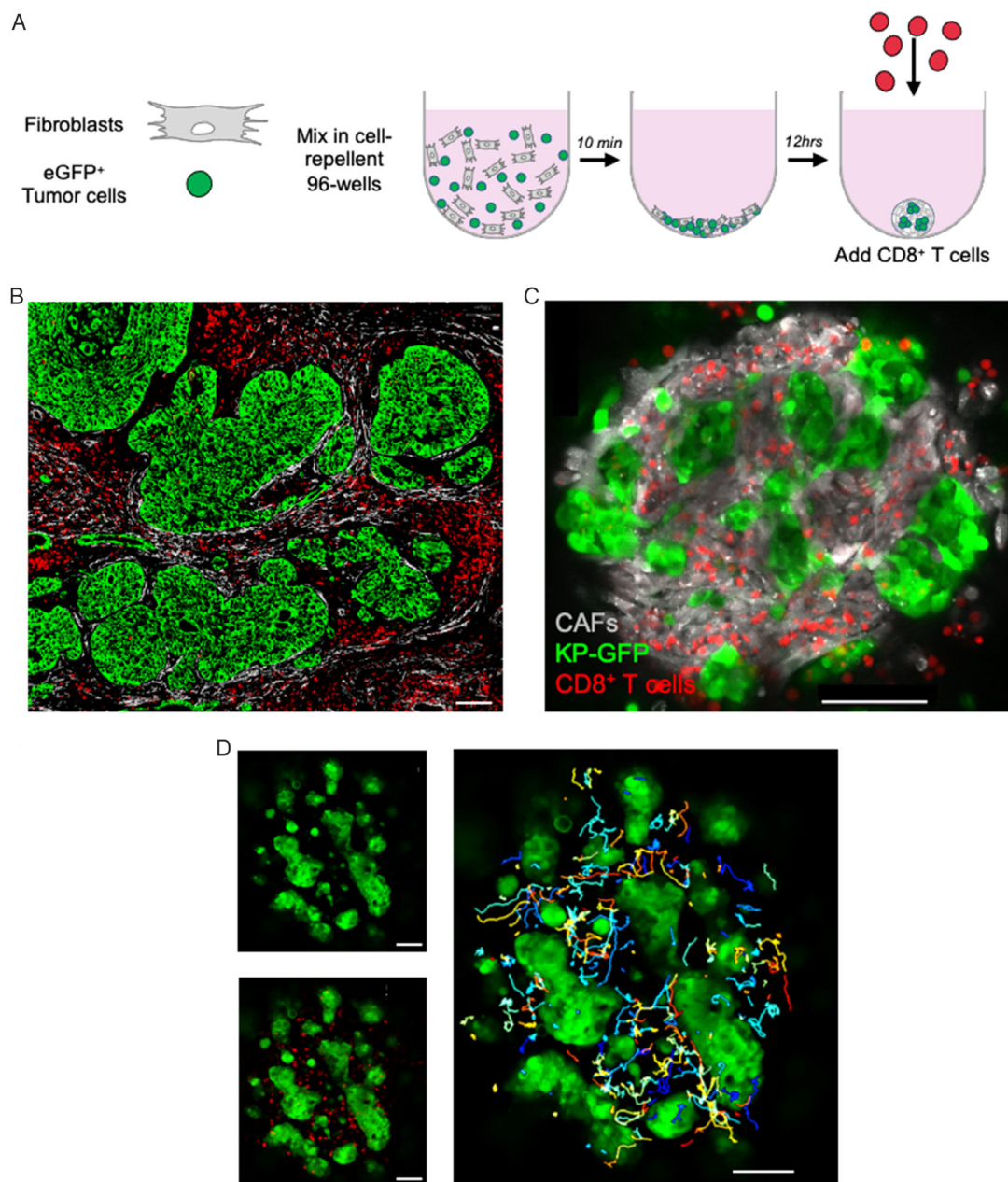


Figure 2. Murine lung tumor spheroids allow evaluation of lymphocyte infiltration and motility. A) Schematic representation of protocol for CD8⁺ T-cell monitoring. B) Multiplexed immunohistochemical staining, performed on a formalin-fixed, paraffin-embedded human lung cancer patient biopsy. Sequential immunostainings for keratin (tumor cells, green), CD3 (grey) and α -SMA⁺ CAFs (red) were overlaid in pseudofluorescence. C and D) Confocal live images of a representative KP spheroid composed of 30 k eGFP⁺ KP cells (green) and 50 k mCherry⁺ CAFs (grey, not in panel D) with 50 k cell trace violet (CTV) labelled CD8⁺ OT-I T cells (red). C) Images were created at $\approx 40 \mu\text{m}$ depth, 24 h after spheroid generation and 12 h after CTV-labelled CD8⁺ OT-I T cell addition. D) Representative Z-projection (24 μm thick, 6 slices) from a 36 min video (Video S1, Supporting Information) tracking polyclonal CD8⁺ T-cell motility in a KP-CAF spheroid. Top left: KP tumor islets only, bottom left: T cells (red) merged on top, and right: multicolor T-cell tracks (length $>10 \mu\text{m}$) as tracked with the TrackMate ImageJ plugin. Scale bars represent 100 μm in all images.

infiltrate in the stroma between but not in the tumor islets (Figure 2B). Interestingly, upon addition of preactivated cell trace violet (CTV) labelled CD8⁺ T cells to freshly formed spheroids ($t = 12$ h) at a KP:CAF:CTL ratio of 3:5:5, we show through live cell confocal imaging that the majority of T cells also localized in the stroma adjacent to tumor cell islets as soon as 16 h after T cell addition (Figure 2C). In addition, we captured live confocal Z stack videos to track T cell motility (Figure 2D and Video S1, Supporting Information), allowing quantitative readouts of T-cell speed, directionality, and number of tumor–T-cell contacts.

In the context of lung tumor-infiltrating myeloid cells, TAMs have been shown to play an ambiguous role in cancer progression.^[44] Both extremes of their polarization spectrum are defined as inflammatory, tumoricidal MHC-II^{high} “M1-like” versus alternatively activated, immunosuppressive and protumoral MHC-II^{low} “M2-like” TAMs.^[14,45] To compare the infiltration profile between M1-like and M2-like TAMs, we generated bone-marrow-derived macrophages, polarized for 24 h with IFN- γ or IL-4 respectively. Three hours after KP or LLC spheroids were formed ($t = 3$ h), M1- or M2-like macrophages were added at a 3:1 tumor:macrophage ratio. Three days later, spheroids were fixed, cryosectioned, stained for F4/80 and imaged to assess macrophage localization. While M2-like macrophages showed a preference to infiltrate in KP spheroids (Figure 3A,B) over the M1-like macrophages, both macrophage types

penetrated relatively evenly into LLC spheroids (Figure 3C). To investigate the impact of CAFs on their respective infiltration pattern, we also generated KP and LLC spheroids with twice the amount of CAFs. Notably, this further strengthened the observation in KP spheroids that M2-like TAMs show a more pronounced tendency to infiltrate into the KP spheroids than their M1-like counterparts (Figure 3D). Notably, the opposite seems to hold true for the LLC spheroids with twice the amount of CAFs, as the M2-like TAMs were found more frequently at the spheroid border while the M1-like TAMs showed a more evenly distributed infiltration profile (Figure 3E). These findings highlight the tumor cell type as well as the tumor to CAF ratio significantly and differently impact the capacity of M1- and M2-like TAMs to penetrate the TME.

2.3. 3D Spheroid Killing Assay Allows T-Cell-Mediated Target-Specific Killing Assessment

Aside from oncoimmunology models to enhance our understanding of the lung TME, high-throughput assays to assess CTL-mediated target cell-specific killing are also needed. Especially in the framework of ICI and chimeric antigen receptor (CAR) T-cell evaluation.

To design a target cell-specific 3D killing assay, we generated eGFP⁺ target and Kat⁺ nontarget derivatives of the LLC, KP, and

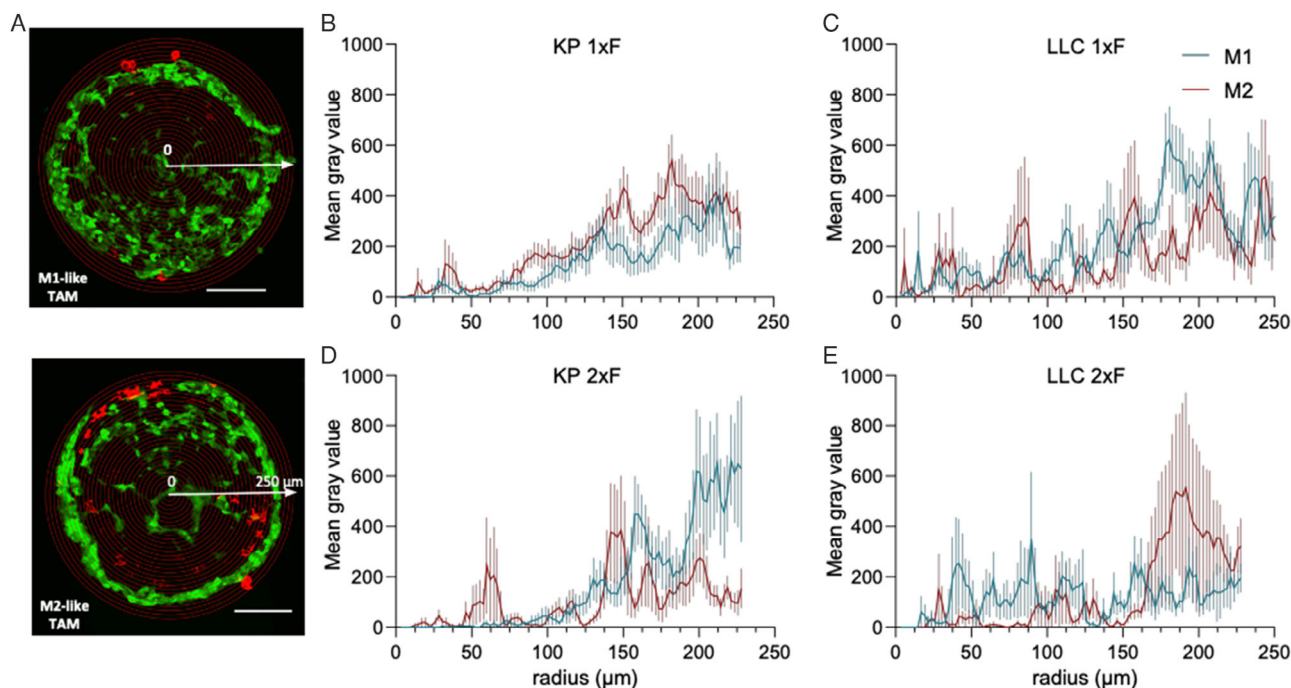


Figure 3. M1- and M2-like TAMs within KP and LLC spheroids with different tumor to CAF ratio show different infiltration profiles. A) Three hours after 3 k eGFP⁺ KP or 6 k eGFP⁺ LLC or were mixed with 5 k fibroblasts, 1 k or 2 k M1- or M2-like macrophages (red) were added respectively to obtain a 3:1 tumor to macrophage ratio. Another 3 days later, spheroids were washed, formalin fixed, cryosectioned, and stained for F4/80⁺ macrophages (red). A) eGFP⁺ green signal of KP spheroid mixed with M1 macrophages (top, red) or M2-like macrophages (below, red). To visualize infiltration analysis, an overlay of concentric circles ranging from the center till the spheroid border (250 μ m) is depicted. On each circle, the mean gray value of the macrophage signal is measured. Scale bars represent 100 μ m. B and C) Mean gray values representing F4/80⁺ macrophages' penetration profile into KP and LLC spheroids (3D 1xF). D and E) Mean gray values representing F4/80⁺ macrophages' penetration profile into KP and LLC spheroids with twice the amount of CAFs (3D 2xF). Mean gray values were determined via ImageJ on whole-mount confocal images of 3 days old KP and spheroids, plotted as mean \pm SD ($n = 1$ –2, 6–9 replicates per condition).

H1650 lines. The target was chosen based on the antigen recognized by the CTL delegate. In case of the murine 3D killing assays, the latter was represented by CD8⁺ T cells, isolated from transgenic OT-I mice, described to have a T-cell receptor that specifically recognizes the MHC-I molecule H2-Kb that presents the SIINFEKL epitope of ovalbumin (OVA). As a human CTL delegate, the L2D8 melanoma infiltrating lymphocyte clone was chosen, previously described to be directed against a gp100-derived peptide_{209–217} in complex with HLA-A2. The gp100 or melanocyte protein PMEL itself is 661 amino acids long and is considered a typical tumor associated antigen for melanoma. Using different fluorescent markers, their ratio can be followed over time with incucyte live cell imaging and/or flow cytometry as measurement of target cell-specific killing (Figure 4A,B). Hence, we generated an eGFP⁺ and OVA⁺ target KP and LLC line, an eGFP⁺ and gp100⁺ H1650 line next to an mCherry⁺ or Kat⁺ nontarget KP, LLC and H1650 line.

As a proof-of-concept for the 3D killing assay, we measured and compared OT-I-mediated KP target cell-specific killing between spheroids and their 2D monolayer counterparts. Additional variables included: 3D cultures without CAFs (3D noF), twice the amount of CAFs (3D 2xF) and CTLs which were

prestimulated for 1 or 3 days. Three days later, target cell specific killing was measured using flow cytometry showing significantly less efficient killing of one-day prestimulated CTLs in 3D spheroids compared with 2D cultures but not if 3-day prestimulated CTLs were used (Figure 4C). Interestingly, the lack of CAFs counterintuitively reduced the capacity of T cells to kill 3D-cultured target KP (and target LLC, data not shown). Finally, only within spheroids that comprised KP cells and CAFs, differences in T-cell prestimulation showed an impact on their capacity to kill KP target cells, highlighting the importance of CAFs in our model to evaluate the capacity of T cells to kill target cells specifically.

When LLC spheroids were formed in the presence of 5 k M1- or M2-like macrophages, the 3D killing assay was able to confirm a more tumoricidal role for M1-like TAMs, suggestive for the assays' potential to assess the impact of specific immune cell subsets on target cell-specific killing (Figure 4D). Notably, the percentage of LLC target killing by 3-days prestimulated OT-I cells on the "no M" LLC spheroids seemed to be twice as high as compared the percentages obtained during other LLC killing assays, performed at similar conditions (same prestimulation and E:T ratio as depicted in panels A, C, and E of Figure 5).

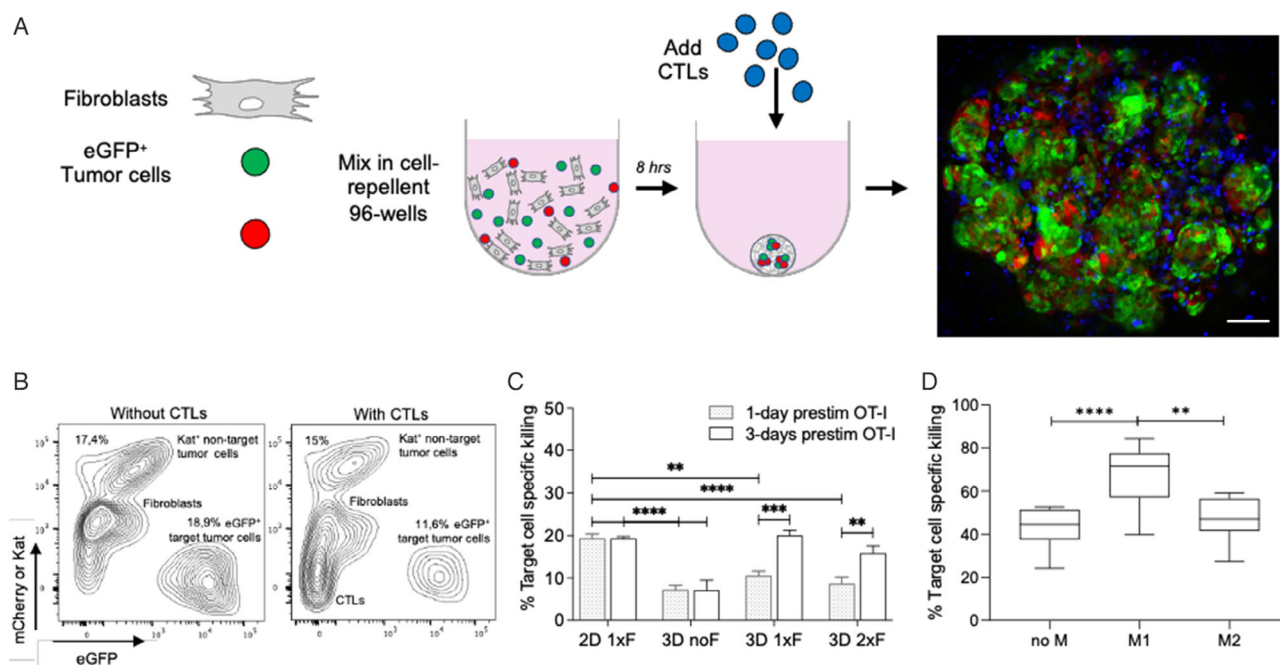


Figure 4. Proof-of-concept of the 3D spheroid killing assay. A) Schematic representation of 3D spheroid killing assay where eGFP⁺ target cells are mixed with mCherry or Kat⁺ nontarget cells and fibroblasts, 8 h before addition of prestimulated CTLs. Right: Representative confocal Z-projection of 24 h-old KP spheroid at $\approx 60 \mu\text{m}$ depth, composed of 15 k target KP-eGFP, 15 k nontarget KP-mCherry, 50 k nonfluorescent fibroblasts and 50 k CTV-labeled prestimulated OT-I cells. Scale bar represents 100 μm . B) Contour plots of LLC spheroid derived single cell suspensions, 3 days after the addition (right) or not (left) of 1.5 k prestimulated OT-I cells. The percentage of target-specific killing, normalized for the eGFP/Kat ratio in spheroids without OT-I cells, is calculated as follows: $1 - (\% \text{ eGFP}^+ \text{ cells} / \% \text{ Kat}^+ \text{ cells}) \text{ with CTLs} / (\% \text{ eGFP}^+ \text{ cells} / \% \text{ Kat}^+ \text{ cells}) \text{ without CTLs}$. C) Histograms represent mean with standard error of the mean of KP target cell-specific killing percentages by 1500 one-day (grey) or 3-days (white) prestimulated OT-I cells, added 8 h after 3 k target KP tumor plating to obtain an effector (E)/target (T) ratio of 0.5. On the x-axis the following four culture conditions can be distinguished: 3 day old KP-fibroblast cocultures in flat bottom plates at 3 k target KP: 3 k nontarget KP: 10 k CAF ratio (2D), KP target cells grown as 3D monoculture in an ULA round bottom plate (3D noF), "normal" K spheroids at 3 k target KP: 3 k nontarget KP: 10 k CAF ratio (3D 1xF) and KP spheroids with 3 k target KP: 3 k nontarget KP: 20 k CAF ratio (3D 2xF) ($n = 2, 5$ replicates/experiment, unpaired t -test gives rise to $p = 0.0004$). D) Target cell-specific killing measured in LLC spheroids in presence or absence of M1- or M2-like macrophages, three days after OT-I CTLs were added ($n = 3, 3-4$ replicates per experiment). Statistical analysis was performed with a Tukey's multiple comparisons one-way ANOVA test.

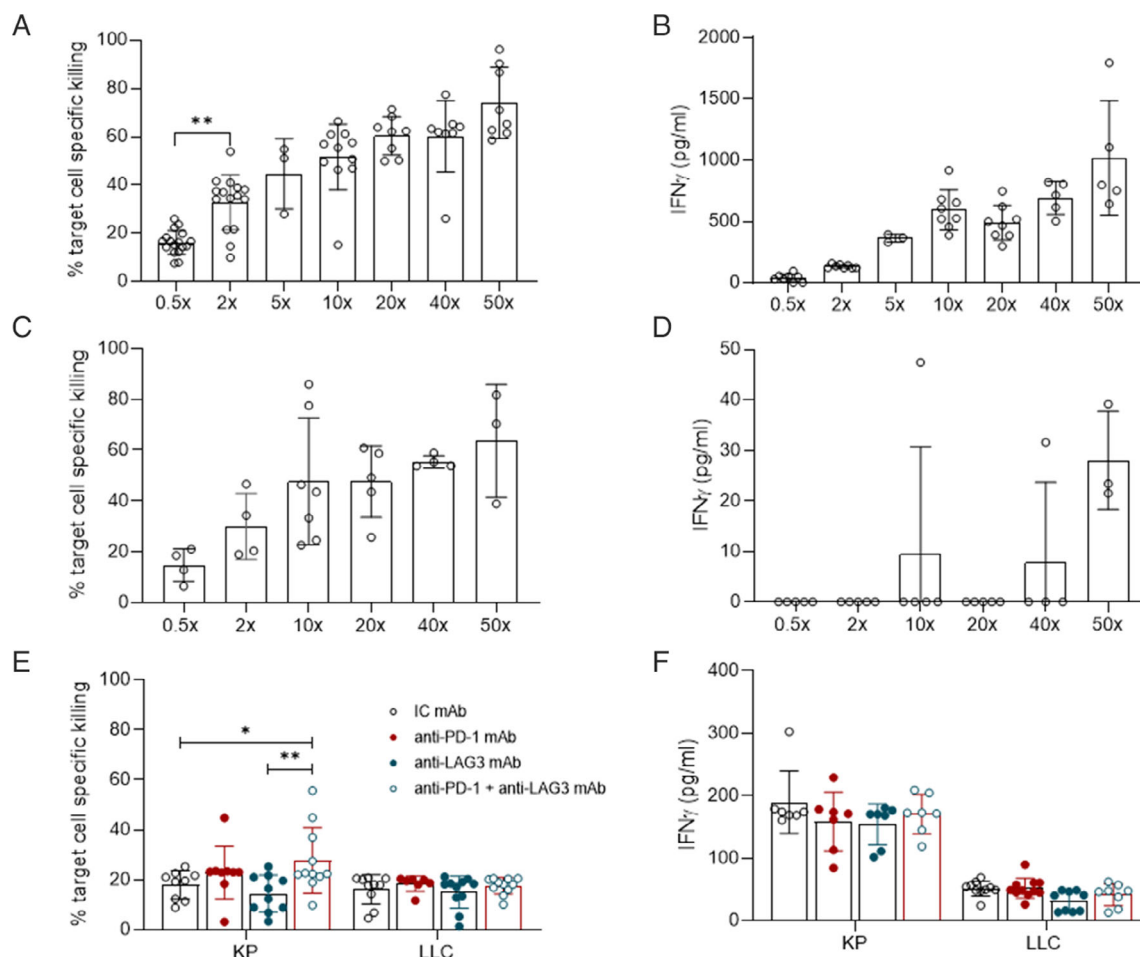


Figure 5. The murine and human 3D spheroid killing assay allow sensitive and spatio-temporal evaluation of CTL-mediated killing. A) Calculated percentages of LLC target specific killing three days after the addition of prestimulated OT-I CTLs at the depicted ratios of E:T (effector CTL over eGFP⁺ target LLC) ($n = 4$, 2-5 replicates/experiment). B) Murine IFN- γ concentrations present in the supernatant at the third day of target cell specific LLC killing by OT-I cells at the depicted E:T ratios ($n = 2$, 3-5 replicates/experiment). C) Calculated percentages of H1650 target specific killing five days after the addition of prestimulated L2D8 CTLs at the depicted E:T ratios ($n = 2$, 2-5 replicates per condition). D) Human IFN- γ concentrations from the respective H1650 spheroids at the fifth day of target cell-specific killing ($n = 1$, 3-5 replicates/experiment). E) Eight hours after LLC and KP spheroid formation, 1500 3-days prestimulated OT-I cells were added together with 5 $\mu\text{g mL}^{-1}$ anti-PD-1 mAb and/or anti-LAG-3 mAb or isotype control IgG2b (IC mAb). Three days later, killing efficacy was recorded after enzymatic digestion of the spheroids using flow cytometry ($n = 3$, 1-6 replicates/experiment). F) Murine IFN- γ concentrations within the supernatant from the respective murine spheroids, collected on the third day of target cell-specific killing ($n = 3$, 1-5 replicates/experiment). A one-way ANOVA with Tukey's multiple comparisons test was performed to determine statistical significance in panels A-F. G) and H) Spatiotemporal follow-up of eGFP⁺-LLC and -H1650 specific target cell killing at a 40:1 or 20:1 E:T ratio, where E is represented by 3-days prestimulated OT-I or L2D8 CTLs respectively. Timeline starts at moment spheroids are generated. Follow-up of one representative spheroid per condition is shown per row, followed over the course of 6 days.

This is explained by the fact that a different batch of OT-I mice was used and warrants to take interexperiment variation into account and only compare differences between conditions within experiments.

To determine the sensitivity of the murine and human 3D killing assay, we subjected LLC and H1650 spheroids to the following E:T ratio's: 0.5; 2; 5; 10; 20; 40; and 50 with 3-days prestimulated OT-I or L2D8 cells, respectively. Three days later, the murine LLC spheroid (Figure 5 A) as well as the human H1650 spheroid (Figure 5C) killing assay showed a stepwise increase in target cell-specific killing in line with the E:T ratio rise. In addition, their supernatants were collected to perform a murine and

human IFN- γ ELISA, respectively. While concentrations of murine IFN- γ showed a similar stepwise increase (Figure 5B), this was less pronounced for the human H1650 killing assay (Figure 5D). The latter argues for the complementarity of a human 3D killing assay to an IFN- γ ELISA when target cell-specific killing evaluation at low E:T is envisaged.

To demonstrate the 3D killing assays' potential for antitumor immunotherapy research, target specific killing was measured using KP and LLC spheroids in the presence of 5 $\mu\text{g/mL}$ anti-PD-1 monoclonal antibody (mAb) and/or mAb that targets the alternative checkpoint molecule Lymphocyte-activation gene 3 (LAG-3). While three days later, LLC target-specific killing

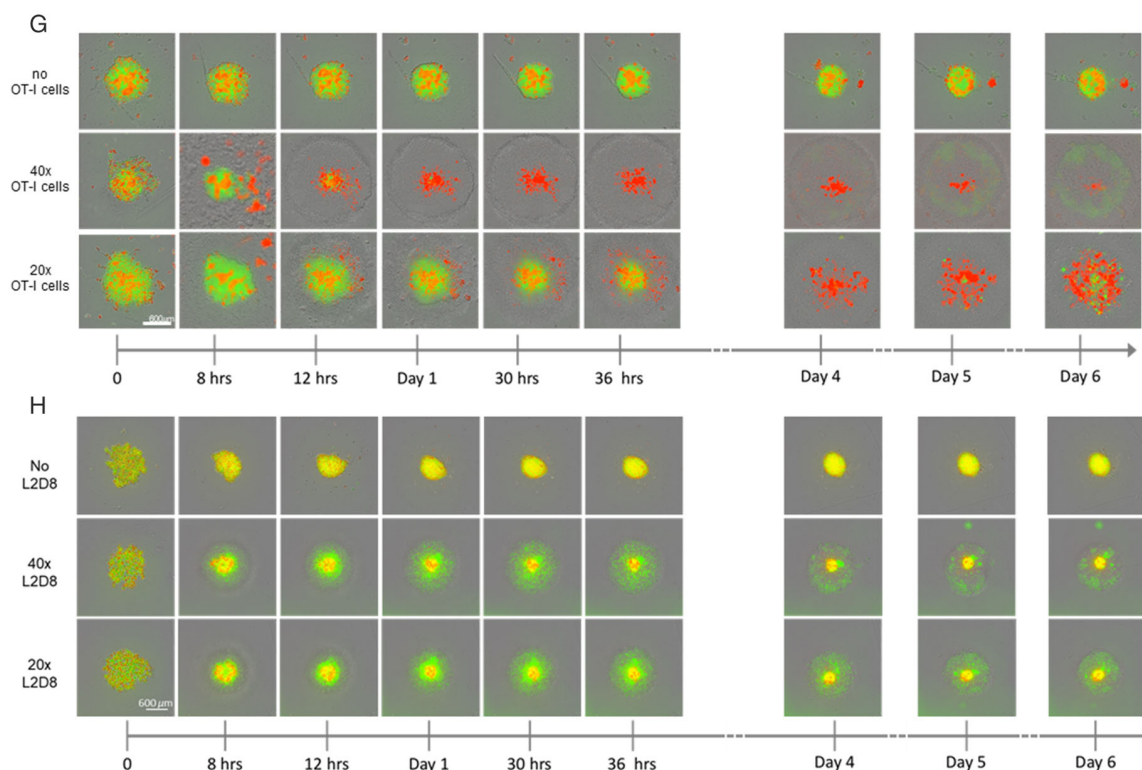


Figure 5. Continued.

remained unchanged, the killing potential of prestimulated OT-I CTLs did significantly change in the KP spheroids. More precisely, a significantly increased KP killing percentage was observed in the presence of the anti-PD-1/anti-LAG-3 mAb combination.

Finally, we evaluated if the murine and human 3D spheroid killing assay could be used to measure the spatio-temporal impact of different E:T ratios. More specifically the difference between an E:T ratio of 20:1 and 40:1 was followed over the course of 6 days on LLC and H1650 spheroids using incucyte live cell imaging, showing a reduction of eGFP⁺ signal over time when OT-I or L2D8 cells were added (Figure 5G,H). Moreover, all spheroids under CTL-attack showed spatial widening, suggestive for T cell infiltration with concomitant ECM disruption. Notably, while flow cytometric analysis of the 20:1 and 40:1 E:T ratio's after 3 days did not show a significant difference in target cell-specific LLC killing, incucyte live cell imaging did reveal some striking differences. Although the 40:1 E:T ratio resulted in complete elimination of eGFP⁺ LLC signal within 24 h, it took the 20:1 E:T ratio more than 3 days to result in a similar pattern (Figure 5G). Moreover, the eGFP⁺ signal reappeared specifically with the 20:1 condition, suggesting that the likelihood to install CTL killing resistance is higher in the presence of a suboptimal amount of CTLs.

3. Discussion

With a growing interest in immunotherapies to treat cancer, suitable oncoimmunology models that allow high-throughput

screenings for predictive biomarkers and novel targets, are needed. In solid cancers like NSCLC, tumor cells continuously interact in 3D with their surrounding TME, composed of non-malignant structural and cellular players. Hence, different 3D culturing methods have been developed to mimic this multicellular profile, ranging from spheroids to organoids and microfluidic systems.^[21] In order to provide an extracellular framework, matrigel is most often used because of its straightforward protocol with high-throughput potential.^[46] However, matrigel embedded 3D models most often lack natural stromal components like ECM, fibroblasts and immune cells, hampering relevant preclinical immunotherapy screening. To meet this gap, we optimized an uncomplicated protocol to generate murine and human lung cancer spheroids in which the *in vivo* human NSCLC tumor-stroma architecture is recapitulated to allow immunotherapeutic research as well as 3D drug screening in 96-well format.

Our straightforward tumor spheroid generation protocol is based on preparing a mixture of syngeneic fibroblasts with fluorescently labelled lung tumor cells at an optimized ratio per cell line. To deliver a proof-of-concept, we opted for two murine and two human NSCLC lines: KP and LLC next to PC-9 and H1650, respectively. Growth kinetic profiles of the different spheroids showed that the surface areas remained stable (LLC) or even decreased (KP and H1650) in the first 5–10 days after formation. These findings are in line with the observation that the addition of a stromal component enhances cancer cell adherence by strengthening cell–cell contacts and tight junctions resulting in compact aggregates.^[47] Moreover, cancer cell line aggregates have been shown to display a significantly slower growth profile compared with their 2D cell culture counterparts.^[48] Notably, we

were unable to obtain rigid spheroids with the human PC-9 line at any tested tumor:fibroblast ratio. According to Han et al., cancer cells' tendency to form compact spheroids or loose cell aggregates is linked to their respective E-cadherin^{high} or N-cadherin^{high} expression. Hence, they recommend using a scaffold-based technique like matrigel for E-cadherin^{low} cancer cells to form rigid spheroids.^[49] During the exponential growth phase of the KP, LLC, and H1650 spheroids, we further observed an increase in spheroid diameter variation. This is in accordance with a previous study that linked this phenomenon to the changing cancer cell:fibroblast ratio over time, suggestive for an optimal spheroid evaluation window between day 1 and 10.^[50]

By incorporating natural ECM-secreting lung fibroblasts, we were further able to demonstrate that the KP, LLC and H1650 spheroids showed a clinically relevant architecture with fibronectin⁺ ECM, deposited by α -SMA⁺ CAFs. Likewise, Amann et al. were able to show fibronectin expression upon co-cultivation of the A549 and Colo699 NSCLC lines with SV-80 lung fibroblasts via a scaffold free hanging-drop method.^[50] By comparing the tumor-stroma organization of the different spheroid types, we observed a clear demarcation between eGFP⁺ tumor cell islets and fibronectin⁺ ECM deposited by α -SMA⁺ CAFs within the KP spheroids. While a similar, yet less pronounced architecture was found within H1650 spheroids, LLC spheroids displayed a more dispersed tumor:CAF profile with less pronounced ECM. In contrast to the unambiguous epithelial origin of the KP and H1650 adenocarcinoma lines, LLC cells have a reported tendency to show a mesenchymal profile.^[41,51,52] Together with the observation that tumor cells can show increased epithelial to mesenchymal transition (EMT) when co-cultured with fibroblasts, suggests that we were able to reveal the LLCs' EMT profile within our LLC spheroids.^[50]

Aside from their usefulness to investigate cancer-stroma interactions, we validated the murine lung tumor spheroids' potential to serve as a versatile arena for the evaluation of immune cell behavior. First, we validated the spheroids potential to study relevant T-cell infiltration and motility, by adding prestimulated OT-I CD8⁺ T cells to 12 h-old KP spheroids. Interestingly, T cells were found to localize in close proximity to CAFs in between the tumor nests and as such correspond nicely to the T cell excluded profile found in NSCLC patient biopsies. Hence our model can serve the preclinical immunotherapy research field, especially in the context of adoptive T cell transfer studies with chimeric antigen receptor (CAR)-modified T and NK cells. While the latter have shown astonishing clinical successes against B-cell malignancies, continuous efforts to translate their success to solid tumors are being hampered by structural and immunosuppressive barriers, characteristic for the multicellular TME of solid cancers.^[53–55] Moreover our 3D lung spheroid generation protocol can serve as a blueprint for the generation of other solid cancer spheroid models.^[54,55] Second, we validated our 3D lung spheroid model to study macrophage infiltration. Clinical studies have suggested that the density of the protumoral M2-like macrophages is associated with a poor prognosis in almost all human cancer types, including lung cancer.^[56–58] To investigate if our model allowed evaluation of TAM subset specific infiltration differences, we compared the infiltration profile of antitumor M1-like TAMs with protumor M2-like TAMs in 3-day old KP and LLC spheroids with different tumor

to CAF ratios. We found that all TAMs tended to penetrate better into LLC spheroids than KP spheroids, arguing for the ECM-hampering role of the KP spheroids for TAM infiltration. Notably, we further observed that M2-like protumoral TAMs were found to penetrate deeper into KP and LLC spheroid cores but that an enhanced CAF to tumor cell ratio shifted this pattern specifically within the LLC spheroids. Although, M2-like TAMs have been shown to reside in more close proximity to hypoxic regions within the TME than their M1-like counterparts,^[59,60] we were unable to evaluate this feature as our 3-day old KP and LLC spheroids did not show an hypoxic core yet (data not shown). To recapitulate, our data do reveal that the type of tumor cell line and tumor to CAF ratio are of decisive importance for TAM infiltration.

Most immunotherapeutics that are preclinically tested for NSCLC today, focus on drugs that unleash NSCLC-specific CD8⁺ T cells that were previously primed by the patients' own adaptive immune system. Yet, these CD8⁺ T cells can only lyse cancer cells after their T-cell receptor is triggered by a specific epitope, presented via a syngeneic major histocompatibility type I (MHC-I) molecule on the cancer cells. Hence, suitable 3D immunotherapeutic drug screening platforms should be histocompatible and provide a read-out for target cell-specific killing.^[61] Today, IFN- γ secretion next to spheroid size decrease are often used to measure CTLs activity and cytotoxicity on tumor suspensions cultured in ULA plates.^[62,63] However, these read-outs do not deliver accurate information on target cell specific killing. In this study we tweaked our lung tumor spheroid model to allow 3D target cell specific killing assessment by introducing a target antigen into the eGFP⁺ KP, LLC, and H1650 lines that is recognized by specific T cells. By mixing these target cells with their red fluorescently labelled nontarget counterparts, the green/red signal served as a sensitive read-out for 3D CTL-mediated target cell specific killing that could be monitored over time using flow cytometry and incucyte live cell imaging.

To deliver a proof-of-concept of the 3D killing assay, we first compared the capacity of one-day and 3-days prestimulated CTLs to kill target cells when grown as tumor:CAF 2D monolayers in flat bottom wells or as 3D lung cancer spheroids in ULA wells with no and twice as many CAFs. While the suboptimally prestimulated CTLs showed a significantly reduced capacity to kill target cells within 3D spheroids compared to 2D tumor:CAF co-cultures, no difference was observed for the 3-days prestimulated CTLs. That the suboptimally prestimulated CTLs were more hampered by the 3D TME, suggests that they experience more hindrance from the deposited ECM, increased cell-cell contacts and tight junctions^[64,65] than their optimally stimulated CTL counterparts. Moreover, tumor-CAFs crosstalk has been shown to mold tumors into a CTL hostile milieu, amongst others by CAF-mediated TGF- β signaling next to the support of protumoral M2-like TAM polarization.^[19,47,66,67] In addition, our 3D lung tumor spheroid killing assay validated that the tumoricidal M1- but not the immunosuppressive M2-like TAMs, are able to ameliorate CTL-mediated killing. Interestingly, CTL dose-escalation experiments with the 3D LLC and H1650 killing assay, revealed that the stepwise increase in killing percentages was not reflected by their IFN- γ secretion profile. This discrepancy is partly explained by the fact that various other markers, which are not detected with an IFN- γ ELISA, can be indicative

for T-cell cytotoxicity like TNF- α , granzyme B, perforin, FasL, and TRAIL.^[68]

In accordance with previous reports on the usefulness of spheroids to deliver information on ICI penetrance,^[69,70] we applied the 3D killing assay to evaluate the impact of two different ICIs, targeting PD-1 and/or LAG-3 on our two different murine lung tumor spheroids. The LLC spheroid killing assay, did not show any increase in CTL-mediated killing upon any of the tested ICI treatments. Interestingly, several preclinical in vivo LLC therapy studies previously described this ICI irresponsiveness.^[51,71] Moreover, the latter studies showed that not the cancer cells, but the nonmalignant host cells are the main determinants of response to ICI in the context of LLC. Hence our LLC spheroid model could be used to unravel which cell subsets should be included to show a beneficial effect on target cell-specific killing by ICIs. In contrast, CTLs showed a significant amelioration of their target cell-specific killing capacity towards KP cells in the presence of the anti-PD-1 and anti-LAG-3 mAb combination, but not upon anti-PD-1 or anti-LAG-3 monotherapy. An observation that is in line with the previously observed lack of response to anti-PD-1 therapy in KP-bearing mice.^[72] Importantly, the co-expression of PD-1 and LAG-3 on T-cells in, amongst others NSCLC patients, has been linked to resistance to anti-PD-(L)1 therapy.^[73–75] Together with our in vitro killing data, these findings encourage further investigation of PD-1/LAG-3 co-blockade for the treatment of NSCLC.

Finally, we were able to detect a different kinetic profile for the CTL:tumor (E:T) ratio's 20 and 40, although they did show a similar percentage of target cell specific killing after 3 days. What's more, when the suboptimal E:T ratio of 20:1 was used, we observed the reappearance of a target eGFP⁺ LLC clone 5 days after CTL addition and two days after apparent elimination of the eGFP⁺ target fraction, suggesting that this represents a CTL-resistance clone. The latter offers an interesting platform to unravel novel resistance mechanisms to CTL-mediated target cell killing, a highly relevant research field to ameliorate the sobering response rates that are currently found for immunotherapy in NSCLC patients.^[1,2,76,77]

4. Conclusion

We report on a murine and human lung tumor spheroid platform to evaluate heterogenous cell–cell, cell–ECM, and cell–drug interactions that influence the overall response to immunotherapies and vice versa. The usage of a scaffold free cultivation method in 96-well plates makes it compatible with standard liquid handling equipment. As such this platform represents a straightforward and accessible model for high-throughput screening to serve the exciting yet rapidly evolving field of oncoimmunological gene, cell, and drug discovery.

5. Experimental Section

Animals: Transgenic OT-I mice were purchased from Charles River and bred in house. All animals were handled according to the institutional guidelines and experiments were approved by the Ethical Committee for use of laboratory animals of the Vrije Universiteit Brussel (ECD: 20-394-OC1). Organs were isolated from 6 to 12-week-old littermates.

Spleens were isolated for OT-I CD8⁺ T-cell isolation, while bone marrow was isolated for generation of bone marrow derived macrophages.

NSCLC Patients: In collaboration with the Biorepository and Department of Pathology tumor and adjacent noninvolved lung samples were obtained from surgical specimens of patients undergoing resection at the Mount Sinai Medical Center (New York, NY). Informed consent was obtained in accordance with the following protocol reviewed and approved by the Institutional Review Board at the Icahn School of Medicine at Mount Sinai, IRB Human Subjects Electronic Research Applications 10-00472 and 10-00135, and in collaboration with the Biorepository and Department of Pathology.

Cells and Cell Lines: Mouse Lewis Lung Carcinoma (LLC) cells were a kind gift from Prof. Jo Van Ginderachter (CMIM, VUB). The Kras^{G12D}p53^{−/−} (KP) cell line was a kind gift from Prof. Brian Brown (Icahn School of Medicine at Mount Sinai, NY). The human HLA-A2⁺ PC-9 and H1650 lung adenocarcinoma lines were a kind gift from Prof. Jacques De Grève (LMMO, VUB). The human HLA-A2⁺ CCL186 (IMR90) lung fibroblast line and Human Embryonic Kidney 293T (HEK293T) cells were obtained from ATCC. Murine LLC and HEK293T cells were maintained in Dulbecco's Modified Eagle's Medium (DMEM, Sigma-Aldrich). Murine KP cells were kept in Iscove's Modified Dulbecco's Medium (IMDM, Thermo Scientific) while the human H1650 and CCL186 lines were maintained in Roswell Park Memorial Institute (RPMI-1640, Sigma-Aldrich) and minimum essential medium (MEM, Gibco) respectively. All media were supplemented with heat-inactivated fetal bovine serum (10%, FBS, TICO), penicillin (100 units mL^{−1}), streptomycin (100 mg mL^{−1}) and L-glutamine (2 mM, Sigma Aldrich). Supplemented media are indicated by a "+", e.g., DMEM+. Cells were cultivated in polystyrene flasks and passaged every 2–3 days to keep confluency at 75%. The L2D8 clone, directed against a gp100-derived peptide_{209–217} in complex with HLA-A2 as described,^[78] was maintained in IMDM (Gibco) with human serum (10%, Innovative Research), IL-2 (30 ng mL^{−1}) (PeproTech), penicillin (100 units mL^{−1}), streptomycin (100 mg mL^{−1}) and L-glutamine (2 mM), referred to as IMDM-L2D8.

Lentiviral Vector Production and Transduction: The REV, GAG, VSV.G packaging, and pCCLsin_hPGK_eGFP-WPRE transfer plasmids were kind gifts from Prof. Brian Brown (Mount Sinai Icahn School of Medicine, NY). After removal of the eGFP sequence from the latter transfer plasmid through a BamHI/Sall restriction digestion, a Katushka or mCherry encoding gBlock with BamHI and Sall overhangs (obtained from IDT) was ligated to obtain the pCCLsin_hPGK_Katushka or mCherry-WPRE transfer plasmid. Furthermore, the transfer plasmids pHR'rip_CMV_huli80tOVA-IRES-tNGFR SIN and pLenti_CMV-gp100-wpre-PGK-puro-DCL-OPT were previously described^[10,11] while the Efla-Large T-antigen_Ires_Puro transferplasmid was obtained via Addgene (Item ID: 18 922). For generation of all third-generation lentiviral vectors (LVs), HEK293T cells were plated at 15 × 1e6 cells per 175 cm² and transfected the next day using polyethylenimine (Polysciences, Eppelheim, Germany) with 6.25; 12.5; 9; and 37.5 μ g of the REV, GAG, VSV.G envelope, and transgene encoding plasmid, respectively. LV-containing supernatant was collected the following 3 days and 1000 \times concentrated by ultracentrifugation as previously described.^[79]

Generation and Validation of Immortalized Murine Fibroblast Line: Lung tissue from one C57BL/6J mouse was perfused with phosphate buffered saline (10 mL, PBS, Sigma Aldrich), isolated and minced into small pieces which were incubated in 20 mL digestion buffer for 45 min at 37 °C. This digestion buffer consisted of NaCl (82.5 mM); Hepes (5.5 mM); CaCl₂ (1.1 mM); Collagenase type I (0.1%) from *Clostridium histolyticum* (Sigma Aldrich) and Dispase II (2.4 U/ml, Sigma Aldrich). Next, minced lung pieces were transferred to a 100 mm tissue culture plate (Falcon) and immersed in DMEM+ (5 mL) with FBS (20%, Biochrom AG). Five days later, viable lung fibroblasts were trypsinized and expanded in a 24-well plate. For immortalization, the primary lung fibroblasts were transduced at multiplicity of infection (MOI) of 10 with LV-LargeTantigen-puro, followed by three puromycin selection rounds at 1 μ g/mL. To confirm their fibroblast identity, fibroblasts and LLC cells were seeded at 1e5 cells in a 6-well plate and 72 h later, single-cell suspensions were generated, snap frozen and stored at −80 °C. RNA extraction was performed using the

RNeasy mini kit (Qiagen), RNA recovery quantified using the nanophotometer (Implen) and cDNA prepared using the Verso cDNA kit (Thermo Fisher Scientific). RT-qPCR was carried out in the Bio-Rad mastermix at the following regimen: 50 °C—2 min; 95 °C—2 min; 40× (95 °C—1 s and 60 °C—30 s) using QuantStudio 12 K Flex (Thermo Fisher Scientific). An overview of the used fibroblast specific primers can be found in Table S1, Supporting Information.

Generation of Target and Nontarget LLC, KP, and H1650 Cell Lines: For the generation of the murine-enhanced green fluorescent protein (eGFP) and ovalbumin (OVA)⁺ Lewis Lung Carcinoma (LLC) and KP target cell lines, 1e5 wild-type cells were first transduced with LVs encoding eGFP and LVs encoding OVA and truncated nerve growth factor receptor (tNGFR) (each at MOI 10). One week later, eGFP and tNGFR double positive cells were sorted using a FACSAria III (BD Biosciences) to obtain the eGFP/OVA-LLC and eGFP/OVA-KP line. The Katushka (Kat)⁺ or mCherry⁺ nontarget LLC and KP lines as well as the mCherry⁺ murine fibroblasts, were generated by transduction with LV-Kat or LV-mCherry and subsequent sort to obtain the Kat-LLC, Kat-KP, and mCherry-fibroblast line. Similarly, the human target and nontarget H1650 lines were generated using LV-eGFP and LV-gp100-puro or LV-Kat resp. After puromycin selection (from 2 to 5 µg mL⁻¹) of the gp100⁺ target line, both the eGFP⁺ target cells and Kat⁺ non-target population were FACS purified.

Murine Bone Marrow-Derived Macrophage Generation and Polarization: Bone marrow from C57BL/6 J OT-I mice was obtained by flushing tibiae and femurs through a 40 µm cell strainer with cold PBS (Sigma-Aldrich). Red blood cells were lysed using 5 mL tris-buffered ammonium chloride for 5 min. Cells were neutralized and seeded at 5 × 1e6 cells/mL in a 10 cm not TC-treated Petri Dish (Corning) with DMEM+ (10 mL). To generate macrophages, murine M-CSF (50 ng mL⁻¹, Immunotools) was added and replenished after 72 h. Macrophage polarization was carried out another 96 h later by incubating the cells for 24 h with M-CSF (5 ng mL⁻¹) with IFN-γ (200 ng mL⁻¹, Immunotools) or IL-4 (40 ng mL⁻¹, Immunotools) for M1-like or M2-like macrophages, respectively, as we previously described.^[80]

Generation of Murine and Human Lung Tumor Spheroids: In general, murine LLC and KP spheroids were generated by mixing 6000 LLC or 3000 KP cells with 5000 immortalized fibroblasts in 100 µL DMEM+ or IMDM+ medium, respectively. Notably, to reproducibly achieve a tumor islet-stroma architecture in the KP spheroids that recapitulates the in vivo human situation, KP cells should be grown to ≈60–80% confluency on the day of spheroid generation. Next, KP cells were washed, and trypsinized for exactly 90 s at 37 °C after which tapping the flask resulted in detachment of cell clumps, crucial for islet formation. Hence after detached cell clumps were washed with prewarmed media, they were collected by carefully pipetting them to ensure maximal clump size before mixing them with fibroblasts.

For human lung tumor spheroids, 6000 H1650 cells were mixed with 5000 CCL186 lung fibroblasts per 100 µL RPMI-1640+ medium. Every spheroid mixture of 100 µL was cultivated in a 96-well CELLSTAR U-shaped cell-repellent plate (650 970, Greiner).

Visualization of T-Cell Infiltration in KP Spheroids: To allow better visualization of T-cell infiltration in the tumor stroma, 10× larger KP spheroids were generated with 30 000 eGFP⁺ KP cells and 50 000 immortalized fibroblasts. To visualize the infiltration and motility of 50 000 viable OT-I T cells, the latter were stained using 5 µM of Cell Trace Violet (CTV, clone: C34557, brand: Invitrogen) prior to their addition to 12 h old KP spheroids. On day later, live spheroid imaging was performed using confocal microscopy.

Visualization of Macrophage Infiltration in LLC and KP Spheroid: For 3D visualization of macrophage infiltration, in vitro differentiated and polarized M1 and M2 polarized macrophages were detached after a 30 min incubation step with 2 mL of Accutase (Sigma Aldrich) at 37 °C. Three hours after spheroid formation, 5500 or 1000 macrophages were added to LLC and KP spheroids, respectively. Another three days later, spheroids were washed, formalin fixed overnight, after which the macrophages were stained within the whole spheroid (so unsliced) as described below.

Confocal Microscopy: Depending on the envisaged outcome, spheroids were imaged via confocal microscopy either live or after fixation (4% paraformaldehyde overnight at 4 °C) and cryosectioning at 5 µm per slide.

Live Cell Imaging: To image T-cell motility in spheroids, they were transferred to CELLview slides (543 079, Greiner Bio-One) and imaged using the environmental control box of Zeiss LSM780, or the Leica TCS SP8 and the Okolab top stage incubator, both at 37 °C, 5% CO₂, 95% humidity. Z-stacks were captured at 4 µm steps until 60–80 µm depth depending on visibility, as live (uncleared) spheroids quickly become too dense for efficient imaging. To maintain sufficiently high framerates (≈30 s per frame) for T cell motility capture, only a partial Z-Stack was selected. For the spatio-temporal follow-up of target cell specific killing, ULA 96-well plates were placed into the IncuCyte Live Cell Imager with 5× objective directly and followed up over the course of 6 days.

Immunohistochemistry on Spheroid Cryosections: Prior to freezing 3 days old, fixed spheroids in Optimal Cutting Temperature compound (OCT, Scigen Inc.), they were consecutively immersed in a 10–20–30% sucrose gradient (2 h at room temperature per gradient). Once embedded and frozen in OCT, cryosections of 12 µm were obtained with the Cryostar NX-50 cryomicrotome. Slices were washed with PBS with 0.1% Tween and subsequently blocked for 1 h in PBS with FBS (4%), bovine serum albumin (BSA, 1%, Sigma-Aldrich) and Tween (0.1%) (blocking buffer). For staining, the anti-α-SMA-Cy3 (clone: C6198, brand: Sigma Aldrich) and anti-fibronectin antibodies (clone: F3648, Sigma Aldrich) were dissolved in blocking buffer to stain the slices overnight, while secondary anti-rabbit IgG AF647 conjugated antibody (clone: 711-605-152, brand: Jackson ImmunoResearch) was incubated on washed slices for 2 h the next day. After a final wash step, slides were air-dried and sealed with a coverslip using Prolong Gold anti-fade reagent (Life Technologies). Images were recorded with a 20× objective on an Axio-Observer Zeiss-LSM 800 or an Axio-Scan N1 instrument (as stated in the figure legends) and analyzed using the Zen 2.6 (blue edition).

Immunohistochemistry on Human Tissue: Formalin-fixed, paraffin-embedded human lung cancer tissues were obtained from the Institut Mutualiste Montsouris. Tissue slides were baked at 37 °C overnight before deparaffinization and rehydration in xylene and ethanol baths, respectively. Heat and pH-mediated antigen retrieval was done in citrate buffer (pH 6 or 9) (Agilent Dako, S2367 or 2369) at 95 °C for 30 min. Endogenous peroxidase activity quenching, protein blocking, primary and secondary antibodies incubations, and revelation using AEC were done manually. Tissues were counter stained with hematoxylin and mounted using a glycerol-based mounting medium (Agilent Dako, C0563). Slides were imaged at 40× with the Hamamatsu NanoZoomer S60 Slide Scanner. Chromogen staining was removed with ethanol before the start of a new antigen retrieval step and immunostaining cycle. Primary antibodies used recognized keratin (clone: AE1/AE3, brand: Agilent), α-SMA (clone: 1A4, brand: Fisher Scientific), CD3 (clone: 2GV6, brand: Roche), and FAP (clone: EPR20021, brand: Abcam).

Image Analysis: Spheroid surface areas were measured using ImageJ. For T-cell motility follow-up, Z-Stacks were reconstructed using ImageJ. Tracking was performed using the Trackmate plugin in ImageJ.^[81] To estimate the penetration profile of macrophages within spheroids, F4/80⁺ cells were located via whole mount confocal imaging. Using the concentric circles plug-in for ImageJ, the entire spheroid area was subdivided in 100 concentric rims with decreasing diameter. The mean gray value on each rim was measured to plot the macrophages infiltration profile.

Target Cell-Specific 3D Killing Assay: Using the CD8a⁺ T-cell Isolation Kit (Miltenyi Biotec), the CD8⁺ T-cell fraction from a freshly isolated OT-I mouse spleen was enriched. Next, 1e6 CD8⁺ OT-I cells per mL RPMI-1640+ with β-mercaptoethanol (50 µmol L⁻¹) were stimulated for three days with 20 µL⁻¹ Mouse T-Activator CD3/CD28 Dynabeads (Gibco). Only for the assays in Figure 4C 1-day prestimulated OT-I cells were generated and used as well. Subsequently, prestimulated OT-I cells were added 8 h after spheroid formation. As a human CTL equivalent, we opted for the L2D8 CD8⁺ tumor infiltrating T-cell clone, specific for the gp100-derived peptide_{209–217} in complex with HLA-A*02. For revival of this T-cell clone, we first co-cultured them for 6 days with 100 Gy irradiated HLA-A*02⁺ gp100⁺ 624mel stimulatory cells and HLA-A2 feeder in IMDM-L2D8 medium supplemented with IL-2 (30 ng mL⁻¹, PeproTech). On the fourth day, medium was replenished with IL-2 (30 ng mL⁻¹). Another two days later, medium was replenished again,

supplemented with IL-2 (30 ng mL⁻¹) and OKT-3 (30 ng mL⁻¹) for stimulation (Clone: BE0001-2, BioXCell). At day ten, CTLs were washed and added to H1650 spheroids, 8 h after H1650 spheroid formation. Target specific killing was measured via flow cytometry at day three (for mouse) or five (for human) after CTLs were added.

Flow Cytometry: To analyze the exact percentage of target cell specific killing, single cell suspensions were generated by incubating the individual spheroids in trypsin with 300 U mL⁻¹ collagenase-I for 30 min at 37 °C. After an additional washing step with PBS containing BSA (1%) and sodium azide (0.02%, Sigma-Aldrich), target cell specific killing was evaluated by comparing the ratio of eGFP⁺ (target) over Kat⁺ (nontarget) cells via flow cytometric evaluation on a LSRFortessa flow cytometer (BD) and analysis using FlowJo 10.5.3 software. The percentage of specific killing normalized for the ratio in spheroids without CTLs (OT-I or L2D8) was calculated with the following equation: $1 - (\% \text{ eGFP/OVA-cancer cell} / \% \text{ Kat-cancer cell})$ with CTLs / $(\% \text{ eGFP/OVA-cancer cell} / \% \text{ Kat-cancer cell})$ without CTLs.

ELISA: Protein levels of murine and human IFN- γ were detected on spheroid supernatants, collected at the third and fifth day of cancer cell specific killing resp. The murine and human IFN- γ ELISA kits (Invitrogen) were used according to the manufacturer's protocol.

Antibodies for In Vitro Immune Checkpoint Blockade: The following recombinant monoclonal antibodies (mAb) were added together with the CTLs to the spheroids to obtain a final concentration of 5 μ g mL⁻¹: rat anti-mouse IgG2b isotype control (IC) mAb (clone: LTF-2, Biolegend), rat antimouse anti-PD-1 mAb (clone: RMP1-14, Biolegend) and/or rat antimouse anti-LAG-3 (clone: C9B7W, Biolegend).

Statistics: The asterisk number in the figures indicates the level of statistical significance as follows: * for $p < 0.05$; ** for $p < 0.01$; *** for $p < 0.001$ and **** for $p < 0.0001$. The statistical test used to determine statistical significance is indicated in the figure legends. Statistical tests were performed using Graphpad Prism v8.3.0.

Supporting Information

Supporting Information is available from the Wiley Online Library or from the author.

Acknowledgements

K.D. and N.T. contributed equally to this work. K.D. and N.T. share first authorship, H.S. and C.G. share last authorship. The authors thank Mathias Van Bulck for his valuable tips and tricks regarding the spheroid stainings and confocal imaging. K.D.R., R.M.A., H.C. and C.G. were supported by Kom op tegen Kanker, Fonds Wetenschappelijk Onderzoek (FWO-V grants 1515718N, G041721N and FWO-SBO grant S004317N), Wetenschappelijk Fonds Willy Gepts of the UZ Brussel, and the BCLAS Fund in honour of Jean Ren   Maisin. C.G. is also an ILC Foundation Awardee supported by the International Association for the Study of Lung Cancer Foundation. J.-T.W., A.B. and H.S. are supported by the Association pour la Recherche sur le Cancer (ARC), Institut Curie, and have received funding from the European Union's Horizon 2020 research and innovation programme under the Marie Sk  łodowska-Curie grant (agreement No 847718).

Conflict of Interest

The authors declare no conflict of interest.

Data Availability Statement

The data that support the findings of this study are available from the corresponding author upon reasonable request.

Keywords

cancer-associated fibroblasts, cytotoxic T-cell infiltration and killing assay, immunotherapy, lung cancer spheroids, oncoimmunology models, tumor infiltrating myeloid cells

Received: September 16, 2021

Revised: November 13, 2021

Published online:

- [1] L. Liu, H. Bai, C. Wang, S. Seery, Z. Wang, J. Duan, S. Li, P. Xue, G. Wang, Y. Sun, X. Du, X. Zhang, Z. Ma, J. Wang, *J. Thoracic Oncol.* **2021**, 16, 1099.
- [2] R. M. Memmott, A. R. Wolfe, D. P. Carbone, T. M. Williams, *J. Thoracic Oncol.* **2021**, 16, 1086.
- [3] L. Paz-Ares, A. Spira, D. Raben, D. Planchard, B. C. Cho, M.   zg  ro  lu, D. Daniel, A. Villegas, D. Vicente, R. Hui, S. Murakami, D. Spigel, S. Senan, C. J. Langer, B. A. Perez, A. M. Boothman, H. Broadhurst, C. Wadsworth, P. A. Dennis, S. J. Antonia, C. Faivre-Finn, *Ann. Oncol.* **2020**, 31, 798.
- [4] D. Yan, Y. Chen, *Sci. Rep.* **2021**, 11, 9020.
- [5] D. Lambrechts, E. Wauters, B. Boeckx, S. Aibar, D. Nittner, O. Burton, A. Bassez, H. Decaluw  , A. Pircher, K. Van den Eynde, B. Weynand, E. Verbeke, P. De Leyn, A. Liston, J. Vansteenkiste, P. Carmeliet, S. Aerts, B. Thienpont, *Nat. Med.* **2018**, 24, 1277.
- [6] Y. Lavin, S. Kobayashi, A. Leader, E-ad D. Amir, N. Elefant, C. Bigenwald, R. Remark, R. Sweeney, C. D. Becker, J. H. Levine, K. Meinhof, A. Chow, S. Kim-Shulze, A. Wolf, C. Medaglia, H. Li, J. A. Rytlewski, R. O. Emerson, A. Solovyov, B. D. Greenbaum, C. Sanders, M. Vignali, M. B. Beasley, R. Flores, S. Gnjjatic, D. Pe'Er, A. Rahman, I. Amit, M. Merad, *Cell* **2017**, 169, 750.
- [7] M. M. Gubin, E. Esaulova, J. P. Ward, O. N. Malkova, D. Runci, P. Wong, T. Noguchi, C. D. Arthur, W. Meng, E. Alspach, R. F. V. Medrano, C. Fronick, M. Fehlings, E. W. Newell, R. S. Fulton, K. C. F. Sheehan, S. T. Oh, R. D. Schreiber, M. N. Artyomov, *Cell* **2018**, 175, 1014.
- [8] A. Mansuet-Lupo, M. Alifano, N. P  cuchet, J. Biton, E. Becht, J. Goc, C. Germain, H. Ouakrim, J.-F. R  gnard, I. Cremer, P. Laurent-Puig, M.-C. Dieu-Nosjean, H. Blons, D. Damotte, *Am. J. Respir. Crit. Care Med.* **2016**, 194, 1403.
- [9] H. Salmon, J. Idoyaga, A. Rahman, M. Leboeuf, R. Remark, S. Jordan, M. Casanova-Acebes, M. Khudoynazarova, J. Agudo, N. Tung, S. Chakarov, C. Rivera, B. Hogstad, M. Bosenberg, D. Hashimoto, S. Gnjjatic, N. Bhardwaj, A. K. Palucka, B. D. Brown, J. Brody, F. Ginhoux, M. Merad, *Immunity* **2016**, 44, 924.
- [10] P. Salmon, V. Kindler, O. Ducrey, B. Chapuis, R. H. Zubler, D. Trono, *Blood* **2000**, 96, 3392.
- [11] B. Stankovic, H. A. K. Bj  rhovde, R. Skarshaug, H. Aamodt, A. Frafjord, E. M  ller, C. Hammarstr  m, K. Beraki, E. S. B  kkevold, P. R. Woldb  k,   . Helland, O. T. Brustugun, I.   ynebr  ten, A. Corthay, *Front. Immunol.* **2019**, 9, 3101.
- [12] A.-P. Ganesan, M. Johansson, B. Ruffell, A. Beltran, J. Lau, D. M. Jablons, L. M. Coussens, *J. Immunol.* **2013**, 191, 2009.
- [13] B. Chen, H. Li, C. Liu, X. Xiang, S. Wang, A. Wu, Y. Shen, G. Li, *PLoS One* **2020**, 15, e0242173.
- [14] R. M. Awad, Y. De Vlaeminck, J. Maebe, C. Goyvaerts, K. Breckpot, *Front. Immunol.* **2018**, 9, 1977.
- [15] A. Bocanegra, G. Fernandez-Hinojal, M. Zuazo-Ibarra, H. Arasanz, M. Garcia-Granda, C. Hernandez, M. Iba  ez, B. Hernandez-Marin, M. Martinez-Aguillo, M. Lecumberri, A. Fernandez De Lascoiti, L. Teijeira, I. Morilla, R. Vera, D. Escors, G. Kochan, *Int. J. Mol. Sci.* **2019**, 20, 1631.

- [16] O. Shani, Y. Raz, L. Monteran, Y. Scharff, O. Levi-Galibov, O. Megides, H. Shacham, N. Cohen, D. Silverbush, C. Avivi, R. Sharan, A. Madi, R. Scherz-Shouval, I. Barshack, I. Tsarfaty, N. Erez, *eLife* **2021**, 10, e60745.
- [17] C. Feig, J. O. Jones, M. Kraman, R. J. B. Wells, A. Deonarine, D. S. Chan, C. M. Connell, E. W. Roberts, Q. Zhao, O. L. Caballero, S. A. Teichmann, T. Janowitz, D. I. Jodrell, D. A. Tuveson, D. T. Fearon, *Proc. Natl. Acad. Sci. USA* **2013**, 110, 20212.
- [18] H. Salmon, R. Remark, S. Gnjatic, M. Merad, *Nat. Rev. Cancer* **2019**, 19, 215.
- [19] S. Mariathasan, S. J. Turley, D. Nickles, A. Castiglioni, K. Yuen, Y. Wang, E. E. Kadel, H. Koeppen, J. L. Astarita, R. Cubas, S. Jhunjunwala, R. Banchereau, Y. Yang, Y. Guan, C. Chalouni, J. Ziai, Y. Şenbabaoğlu, S. Santoro, D. Sheinson, J. Hung, J. M. Giltneane, A. A. Pierce, K. Mesh, S. Lianoglou, J. Riegler, R. A. D. Carano, P. Eriksson, M. Höglund, L. Somarriba, D. L. Halligan, et al. *Nature* **2018**, 554, 544.
- [20] H. Hu, Z. Piotrowska, P. J. Hare, H. Chen, H. E. Mulvey, A. Mayfield, S. Noeen, K. Kattermann, M. Greenberg, A. Williams, A. K. Riley, J. J. Wilson, Y. Mao, R. Huang, M. K. Banwait, J. Ho, G. S. Crowther, L. P. Hariri, R. S. Heist, D. P. Kodack, L. Pinello, A. T. Shaw, M. Mino-Kenudson, A. N. Hata, L. V. Sequist, C. H. Benes, M. J. Niederst, J. A. Engelman, *Cancer Cell* **2021**, 39, 1531.
- [21] A. A. Fitzgerald, E. Li, L. M. Weiner, *Cancers* **2021**, 13, 1.
- [22] S. Herter, L. Morra, R. Schlenker, J. Sulcova, L. Fahrni, I. Waldhauer, S. Lehmann, T. Reisländer, I. Agarkova, J. M. Kelm, C. Klein, P. Umana, M. Bacac, *Cancer Immunol. Immunother.* **2017**, 66, 129.
- [23] S. Nath, G. R. Devi, *Pharmacol. Therapeut.* **2016**, 163, 94.
- [24] Z. Zhang, H. Wang, Q. Ding, Y. Xing, Z. Xu, C. Lu, D. Luo, L. Xu, W. Xia, C. Zhou, M. Shi, W. B. Coleman, *PloS One* **2018**, 13, e0194016.
- [25] G. Gamerith, J. Rainer, J. M. Huber, H. Hackl, Z. Trajanoski, S. Koeck, E. Lorenz, J. Kern, R. Kofler, J. M. Kelm, H. Zwierzina, A. Amann, *Oncotarget* **2017**, 8, 112647.
- [26] D. Rodenhizer, T. Dean, E. D'Arcangelo, A. P. McGuigan, *Adv. Healthcare Mater.* **2018**, 7, 1701174.
- [27] C. Hirt, A. Papadimitropoulos, V. Mele, M. G. Muraro, C. Mengus, G. Iezzi, L. Terracciano, I. Martin, G. C. Spagnoli, *Adv. Drug Deliv. Rev.* **2014**, 79–80, 145.
- [28] H. A. Kenny, M. Lal-Nag, E. A. White, M. Shen, C.-Y. Chiang, A. K. Mitra, Y. Zhang, M. Curtis, E. M. Schryver, S. Bettis, A. Jadhav, M. B. Boxer, Z. Li, M. Ferrer, E. Lengyel, *Nat. Commun.* **2015**, 6, 6220.
- [29] V. Vaira, G. Fedele, S. Pyne, E. Fasoli, G. Zadra, D. Bailey, E. Snyder, A. Faversani, G. Coggi, R. Flavin, S. Bosari, M. Loda, *Proc. Natl. Acad. Sci. USA* **2010**, 107, 8352.
- [30] M. H. Farazmand, R. Rodrigues, J. W. Gardner, J. Charmet, in *Proc. of the Annual Int. Conf. of the IEEE Engineering in Medicine and Biology Society, EMBS, IEEE, Piscataway, NJ* **2019**, pp. 1579–1583.
- [31] R. M. Sutherland, H. R. MacDonald, R. L. Howell, *J. Natl. Cancer Inst.* **1977**, 58, 1849.
- [32] A. Pavesi, A. T. Tan, S. Koh, A. Chia, M. Colombo, E. Antonicchia, C. Miccolis, E. Ceccarello, G. Adriani, M. T. Raimondi, R. D. Kamm, A. Bertoletti, *JCI Insight* **2017**, 2, e89762.
- [33] L. Wallstabe, C. Göttlich, L. C. Nelke, J. Kühnemundt, T. Schwarz, T. Nerreter, H. Einsele, H. Walles, G. Dandekar, S. L. Nietzer, M. Hudecek, *JCI Insight* **2019**, 4, e126345.
- [34] D. Park, K. Son, Y. Hwang, J. Ko, Y. Lee, J. Doh, N. L. Jeon, *Front. Immunol.* **2019**, 10, 1133.
- [35] S. H. Nam, D. Kim, D. Lee, H.-M. Lee, D.-G. Song, J. W. Jung, J. E. Kim, H.-J. Kim, N. H. Kwon, E.-K. Jo, S. Kim, J. W. Lee, *J. Clin. Invest.* **2018**, 128, 5034.
- [36] S. Ullah, K. Seidel, S. Türkkan, D. P. Warwas, T. Dubich, M. Rohde, H. Hauser, P. Behrens, A. Kirschning, M. Köster, D. Wirth, *J. Control. Release* **2019**, 294, 327.
- [37] S. P. Rebelo, C. Pinto, T. R. Martins, N. Harrer, M. F. Estrada, P. Loza-Alvarez, J. Cabeçadas, P. M. Alves, E. J. Gualda, W. Sommergruber, C. Brito, *Biomaterials* **2018**, 163, 185.
- [38] S. W. L. Lee, G. Adriani, E. Ceccarello, A. Pavesi, A. T. Tan, A. Bertoletti, R. D. Kamm, S. C. Wong, *Front. Immunol.* **2018**, 9, 416.
- [39] M. Magan, E. Wiechec, K. Roberg, *Cancer Cell Int.* **2020**, 20, 1.
- [40] J. S. Bertram, P. Janik, *Cancer Lett.* **1980**, 11, 63.
- [41] M. DuPage, A. L. Dooley, T. Jacks, *Nat. Protocols* **2009**, 4, 1064.
- [42] H. Salmon, K. Franciszkiewicz, D. Damotte, M. C. Dieu-Nosjean, P. Validire, A. Trautmann, F. Mami-Chouaib, E. Donnadieu, *J. Clin. Invest.* **2012**, 122, 899.
- [43] D. Jia, M. Yan, X. Wang, X. Hao, L. Liang, L. Liu, H. Kong, X. He, J. Li, M. Yao, *BMC Cancer* **2010**, 10, 1.
- [44] M. F. Wu, C. A. Lin, T. H. Yuan, H. Y. Yeh, S. F. Su, C. L. Guo, G. C. Chang, K. C. Li, C. C. Ho, H. W. Chen, *Cancer Immunol. Immunother.* **2021**, 70, 1435.
- [45] A. Mantovani, S. Sozzani, M. Locati, P. Allavena, A. Sica, *Trends Immunol.* **2002**, 23, 549.
- [46] B. Calpe, W. J. Kovacs, *Expert Opin. Drug Discov.* **2020**, 15, 955.
- [47] J. Kuen, D. Darowski, T. Kluge, M. Majety, *PLoS ONE* **2017**, 12, e0182039.
- [48] T. H. Booi, L. S. Price, E. H. J. Danen, *SLAS Discov.* **2019**, 24, 615.
- [49] S. J. Han, S. Kwon, K. S. Kim, *Cancer Cell Int.* **2021**, 21, 152.
- [50] A. Amann, M. Zwierzina, G. Gamerith, M. Bitsche, J. M. Huber, G. F. Vogel, M. Blumer, S. Koeck, E. J. Pechriggl, J. M. Kelm, W. Hilbe, H. Zwierzina, D. Gullberg, *PLoS One* **2014**, 9, e92511.
- [51] H. Y. Li, M. McSharry, B. Bullock, T. T. Nguyen, J. Kwak, J. M. Pocobutt, T. R. Sippel, L. E. Heasley, M. C. Weiser-Evans, E. T. Clambey, R. A. Nemenoff, *Cancer Immunol. Res.* **2017**, 5, 767.
- [52] Z. Kosibaty, Y. Murata, Y. Minami, T. Dai, J. Kano, R. Matsuoka, N. Nakano, M. Noguchi, *Lab. Invest.* **2019**, 99, 551.
- [53] S. L. Maude, N. Frey, P. A. Shaw, R. Aplenc, D. M. Barrett, N. J. Bunin, A. Chew, V. E. Gonzalez, Z. Zheng, S. F. Lacey, Y. D. Mahnke, J. J. Melenhorst, S. R. Rheingold, A. Shen, D. T. Teachey, B. L. Levine, C. H. June, D. L. Porter, S. A. Grupp, *N. Engl. J. Med.* **2014**, 371, 1507.
- [54] S. Ma, X. Li, X. Wang, L. Cheng, Z. Li, C. Zhang, Z. Ye, Q. Qian, *Int. J. Biol. Sci.* **2019**, 15, 2548.
- [55] P. Dillard, M. Lie, E. Baken, V. H. Lobert, E. Benard, H. Köksal, E. M. Inderberg, S. Wälchli, *BMC Biotechnol.* **2020**, 20, 1.
- [56] L. Cao, X. Che, X. Qiu, Z. Li, B. Yang, S. Wang, K. Hou, Y. Fan, X. Qu, Y. Liu, *Cancer Manage. Res.* **2019**, 11, 6125.
- [57] S. Borowicz, D. R. Principe, M. J. Dorman, A. J. McHenry, G. Sondarva, S. Kumar, V. Ananthanarayanan, P. E. Simms, A. Hess, A. Rana, *PLOS One* **2021**, 16, e0252197.
- [58] F. Xu, Y. Wei, Z. Tang, B. Liu, J. Dong, *Mol. Med. Rep.* **2020**, 22, 4107.
- [59] J. E. Park, B. Dutta, S. W. Tse, N. Gupta, C. F. Tan, J. K. Low, K. W. Yeoh, O. L. Kon, J. P. Tam, S. K. Sze, *Oncogene* **2019**, 38, 5158.
- [60] D. Laoui, E. Van Overmeire, G. Di Conza, C. Aldeni, J. Keirsse, Y. Morias, K. Movahedi, I. Houbracken, E. Schouppe, Y. Elkrim, O. Karroum, B. Jordan, P. Carmeliet, C. Gysemans, P. De Baetselier, M. Mazzone, J. A. Van Ginderachter, *Cancer Res.* **2014**, 74, 24.
- [61] M. Zanon, F. Piccinini, C. Arienti, A. Zamagni, S. Santi, R. Polico, A. Bevilacqua, A. Tesei, *Sci. Rep.* **2016**, 6, 1.
- [62] J. Friedrich, C. Seidel, R. Ebner, L. A. Kunz-Schughart, *Nat. Protocols* **2009**, 4, 309.
- [63] T. Courau, J. Bonnaireau, J. Chicoteau, H. Bottois, R. Remark, L. Assante Miranda, A. Toubert, M. Blery, T. Aparicio, M. Allez, L. Le Bourhis, *J. Immunother. Cancer* **2019**, 7, 74.

- [64] A. Amann, M. Zwierzina, G. Gamerith, M. Bitsche, J. M. Huber, G. F. Vogel, M. Blumer, S. Koeck, E. J. Pechriggl, J. M. Kelm, W. Hilbe, H. Zwierzina, *PLoS One* **2014**, 9, e92511.
- [65] T. Lämmermann, B. L. Bader, S. J. Monkley, T. Worbs, R. Wedlich-Söldner, K. Hirsch, M. Keller, R. Förster, D. R. Critchley, R. Fässler, M. Sixt, *Nature* **2008**, 453, 51.
- [66] A. Chakravarthy, L. Khan, N. P. Bensler, P. Bose, D. D. De Carvalho, *Nat. Commun.* **2018**, 9, 1.
- [67] L. Evans, K. Milward, R. Attanoos, A. Clayton, R. Errington, Z. Tabi, *Biomedicines* **2021**, 9, 302.
- [68] L. Martinez-Lostao, A. Anel, J. Pardo, *Clin. Cancer Res.* **2015**, 21, 5047.
- [69] X. Liu, J. K. Lukowski, C. Flinders, S. Kim, R. A. Georgiadis, S. M. Mumenthaler, A. B. Hummon, *Anal. Chem.* **2018**, 90, 14156.
- [70] A. Rodallec, G. Sicard, S. Giacometti, M. Carré, B. Pourroy, F. Bouquet, A. Savina, B. Lacarelle, J. Ciccolini, R. Fanciullino, *Int. J. Nanomed.* **2018**, 13, 6677.
- [71] H. Lin, S. Wei, E. M. Hurt, M. D. Green, L. Zhao, L. Vatan, W. Szeliga, R. Herbst, P. W. Harms, L. A. Fecher, P. Vats, A. M. Chinnaiyan, C. D. Lao, T. S. Lawrence, M. Wicha, J. Hamanishi, M. Mandai, I. Kryczek, W. Zou, *J. Clin. Invest.* **2018**, 128, 805.
- [72] C. Pfirschke, C. Engblom, S. Rickelt, V. Cortez-Retamozo, C. Garris, F. Pucci, T. Yamazaki, V. Poirier-Colame, A. Newton, Y. Redouane, Y.-J. Lin, G. Wojtkiewicz, Y. Iwamoto, M. Mino-Kenudson, T. G. Huynh, R. O. Hynes, G. J. Freeman, G. Kroemer, L. Zitvogel, R. Weissleder, M. J. Pittet, *Immunity* **2016**, 44, 343.
- [73] M. Zuazo, H. Arasanz, G. Fernández-Hinojal, M. J. García-Granda, M. Gato, A. Bocanegra, M. Martínez, B. Hernández, L. Teixeira, I. Morilla, M. J. Lecumberri, A. F. de Lascoiti, R. Vera, G. Kochan, D. Escors, *EMBO Mol. Med.* **2019**, 11, e10293.
- [74] R. Y. Huang, A. Francois, A. R. McGray, A. Miliotto, K. Odunsi, *OncolImmunology* **2017**, 6, e1249561.
- [75] A. K. Mishra, T. , X. Wang, E. Driver, Z. Chen, X. J. Wang, J. H. Wang, *Oncotarget* **2016**, 7, 81341.
- [76] P. Sharma, S. Hu-Lieskovan, J. A. Wargo, A. Ribas, *Cell* **2017**, 168, 707.
- [77] L. Horvath, B. Thienpont, L. Zhao, D. Wolf, A. Pircher, *Mol. Cancer* **2020**, 19, 1.
- [78] G. Markel, R. Seidman, N. Stern, T. Cohen-Sinai, O. Izhaki, G. Katz, M. Besser, A. J. Treves, R. S. Blumberg, R. Loewenthal, O. Mandelboim, A. Orenstein, J. Schachter, *J. Immunol.* **2006**, 177, 6062.
- [79] C. Goyvaerts, K. De Groeve, J. Dingemans, S. Van Lint, L. Robays, C. Heirman, J. Reiser, X.-Y. Zhang, K. Thielemans, P. De Baetselier, G. Raes, K. Breckpot, *Gene Ther.* **2012**, 19, 1133.
- [80] Y. De Vlaeminck, Q. Lecocq, P. Giron, C. Heirman, X. Geeraerts, E. Bolli, K. Movahedi, S. Massa, S. Schoonooghe, K. Thielemans, C. Goyvaerts, J. A. Van Ginderachter, K. Breckpot, *J. Control. Release* **2019**, 299, 107.
- [81] J. Y. Tinevez, N. Perry, J. Schindelin, G. M. Hoopes, G. D. Reynolds, E. Laplantine, S. Y. Bednarek, S. L. Shorte, K. W. Eliceiri, *Methods* **2017**, 115, 80.